ULTRASOUND NEWS

December 2023

CLINICAL NEWS | ULTRASOUND

Ultrasound model identifies NAFLD patients with advanced fibrosis

Amerigo Allegretto
Dec 6, 2023

Liver fibrosis is a major prognostic factor in NAFLD, making it important to identify patients with advanced fibrosis – also known as metabolic-associated steatohepatitis (MASH). While magnetic resonance elastography shows high performance metrics in fibrosis grades of 2 and above, it has its share of drawbacks. These include its high cost, limited availability, and contraindications.

Sugimoto and colleagues sought to create an accurate model using multiparametric ultrasound to identify NAFLD patients with advanced fibrosis. It tested the model in a prospective study of 65 biopsy-proven NAFLD patients from seven sites.

The researchers found that among the ultrasound markers, shear-wave speed, normalized local variance, and dispersion slope allowed for identification of advanced fibrosis. These included area under the curve (AUC) values of 0.886, 0.805, and 0.79, respectively.

They also found that the most predictive model was the combination of shear-wave speed and normalized local variance with an AUC of 0.908. Additionally, these markers had the highest regression coefficient values in the study, including 2.34 for shear-wave speed and 6.44 for normalized local variance. These indicate a significant association with fibrosis staging.

Finally, the team reported that normalized local variance showed weak correlation with shear-wave speed, suggesting that these markers see different characteristics on liver fibrosis.

CLINICAL NEWS | ULTRASOUND

AI model aids in ultrasound rotator cuff exams

ELSEVIER

Arthroscopy: The Journal of Arthroscopic & Related Surgery

Available online 23 June 2023

In Press, Corrected Proof What's this?

Systematic Review

Artificial Intelligence Aids Detection of Rotator Cuff Pathology: A Systematic Review

Hongwei Zhan M.D. *, Fei Teng M.D. *, Zhongcheng Liu M.D. *, Zhi Yi M.D., Jinwen He M.D., Yi Chen M.D., Bin Geng M.D., Yayi Xia M.D., Ph.D., Meng Wu M.D., Jin Jiang M.D., Ph.D.

Results

A total of 14 articles, comprising 23,119 patients, met the inclusion and exclusion criteria. The pooled mean age of the patients was 56.7 years, and the female rate was 56.1%. The area under the curve (AUC) of the algorithmic model to detect rotator cuff pathology from ultrasound images, MRI images, and radiographic series ranged from 0.789 to 0.950, 0.844 to 0.943, and 0.820 to 0.830, respectively. Notably, 1 of the studies reported that AI models based on ultrasound images demonstrated a diagnostic performance similar to that of radiologists. Another comparative study demonstrated that AI models using MRI images exhibited greater accuracy and specificity compared to orthopedic surgeons in the diagnosis of rotator cuff pathology, albeit not in sensitivity.

Conclusion

The detection of rotator cuff pathology has been significantly aided by the exceptional performance of AI models. In particular, these models are equally adept as musculoskeletal radiologists in using ultrasound to diagnose rotator cuff pathology. Furthermore, AI models exhibit statistically superior levels of accuracy and specificity when using MRI to diagnose rotator cuff pathology, albeit with no marked difference in sensitivity, in comparison to orthopaedic surgeons.

Level of Evidence

Level III, systematic review of Level III studies.

JUM Journal of Ultrasound in Medicine

aium

Case Series

Fetal "Phrygian Cap" Gallbladder: Malformation or Deformation?

Waldo Sepulveda MD, Angela C. Ranzini MD

First published: 29 November 2023 | https://doi.org/10.1002/jum.16382

Waldo Sepulveda was supported by an unrestricted research grant from the Sociedad Profesional de Medicina Fetal "Fetalmed," Chile.

Abstract

A series of five fetuses with a Phrygian cap gallbladder, a condition infrequently reported in the antenatal period, is reported. In all cases, examination of the fetal gallbladder displayed the characteristic folding of the fundus over the body. No associated findings were detected. The gallbladder length was longer than normal in all cases, suggesting that this anomaly could represent a deformity rather than a primary malformation. This might be caused by excessive longitudinal growth of the gallbladder, eventually folding after the fundus reaches the anterior border of the liver and is then diverted laterally by the abdominal wall.

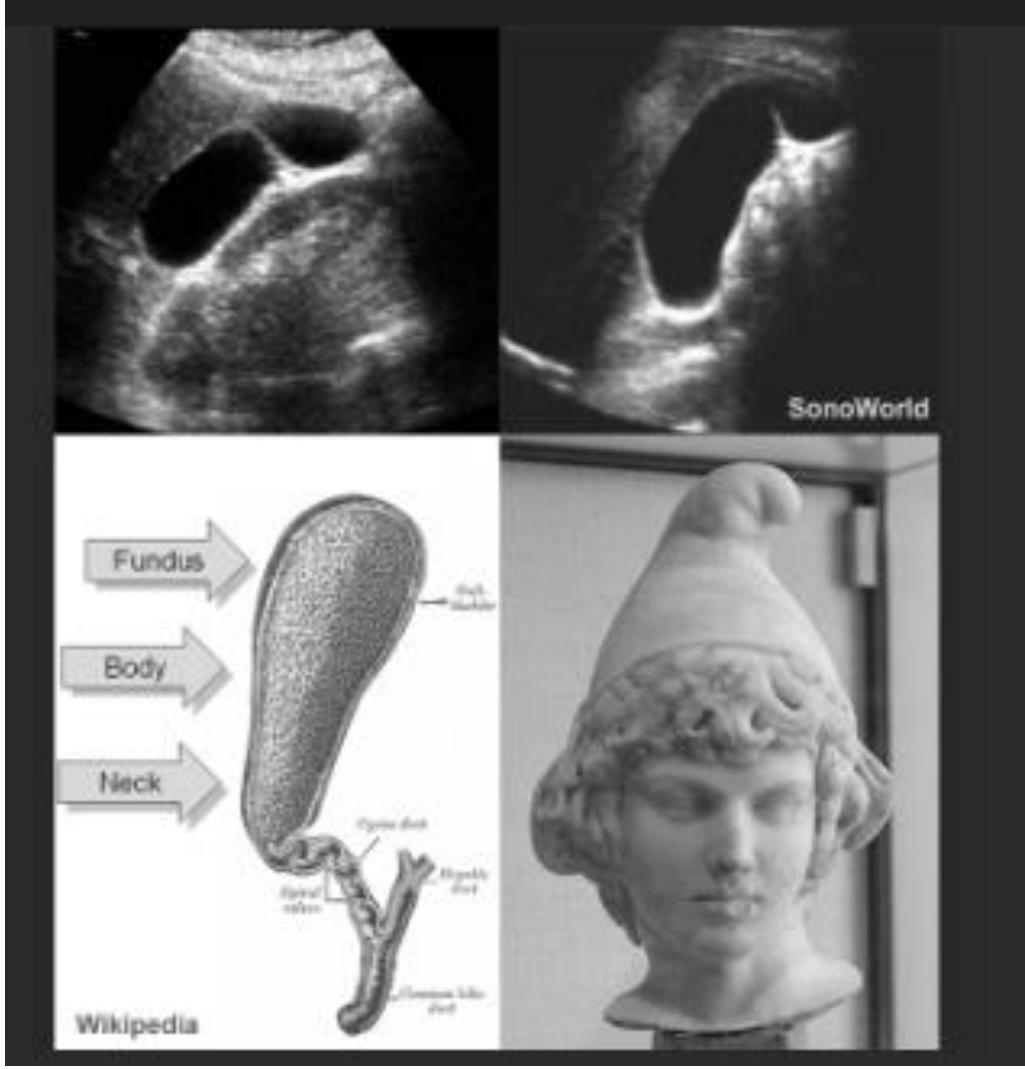

JUM Journal of Ultrasound in Medicine

aium

Pictorial Essay

A Review of Classification, Diagnosis, and Management of Hydrocele

Van Trung Hoang MD, Hoang Anh Thi Van MD, The Huan Hoang MD, Thanh Tam Thi Nguyen MD, Cong Thao Trinh MD

First published: 27 November 2023 | https://doi.org/10.1002/jum.16380

The authors declare no conflicts of interest.

Abstract

This article summarizes and updates a number of issues related to hydrocele including anatomy, embryology, classification, etiology, clinical manifestations, imaging findings, and management. Hydrocele is an abnormal collection of serous fluid between the parietal and visceral layers arising from the mesothelial lining of the tunica vaginalis that surrounds the testis and spermatic cord directly. Hydroceles result from an imbalance of secretion and reabsorption of fluid from the tunica vaginalis. Hydroceles can be divided into two types as primary and secondary. The diagnosis should be based on medical history, clinical manifestations, and imaging studies. Understanding the causes and types of hydroceles is useful for accurately diagnosing and treatment strategy. Hydroceles can be managed by conservative treatment, fluid aspiration, or hydrocelectomy.

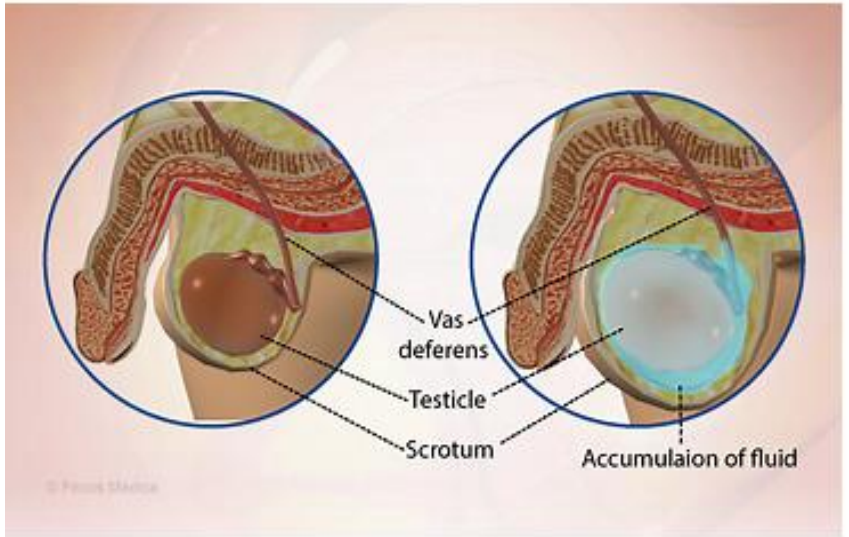

A Novel Prediction Model Based on Quantitative Texture Analysis of Sonographic Images for Malignant Major Salivary Glandular Tumors

CME Credits

Wu-Chia Lo[1,2,3], Ping-Chia Cheng[1,2,4], Wan-Lun Hsu[5], Po-Wen Cheng[1], Li-Jen Liao[1,2,6,7]*

[1]Department of Otolaryngology Head and Neck Surgery, Far Eastern Memorial Hospital, New Taipei, Taiwan, [2]Head and Neck Cancer Surveillance and Research Study Group, Far Eastern Memorial Hospital, New Taipei City, Taiwan, [3]Graduate Institute of Medicine, Yuan Ze University, Taoyuan, Taiwan, [4]Department of Communication Engineering, Asia Eastern University of Science and Technology, New Taipei, Taiwan, [5]Genomics Research Center, Academia Sinica, Taipei, Taiwan, [6]Department of Electrical Engineering, Yuan Ze University, Taoyuan, Taiwan, [7]Biomedical Engineering Office, Far Eastern Memorial Hospital, Taipei, Taiwan

Abstract

Background: The aim of this study was to compare multiple objective ultrasound (US) texture features and develop an objective predictive model for predicting malignant major salivary glandular tumors. **Methods:** From August 2007 to May 2018, 144 adult patients who had major salivary gland tumors and subsequently underwent surgery were recruited for this study. Representative brightness mode US pictures were selected for texture analysis and used to develop a prediction model. **Results:** We found that the grayscale intensity and standard deviation of the intensity were significantly different between malignant and pleomorphic adenomas. The contrast, inverse difference (INV) movement, entropy, dissimilarity, and INV also differed significantly between benign and malignant tumors. We used stepwise selection of predictors to develop an objective predictive model, as follows: Score = 1.138 × Age − 1.814 × Intensity + 1.416 × Entropy + 1.714 × Contrast. With an optimal cutoff of 0.58, the diagnostic performance of this model had a sensitivity, specificity, overall accuracy, and area under the curve of 83% (95% confidence interval [CI]: 74%–92%), 74% (65%–84%), 78% (72%–85%), and 0.86 (0.80–0.92), respectively. **Conclusion:** We have developed a novel computerized diagnostic model based on objective US features to predict malignant major salivary gland tumor. Further improving the computer-aided diagnosis model might change the US examination for major salivary gland tumors in the future.

Keywords: Prediction model, salivary gland tumors, texture, ultrasound

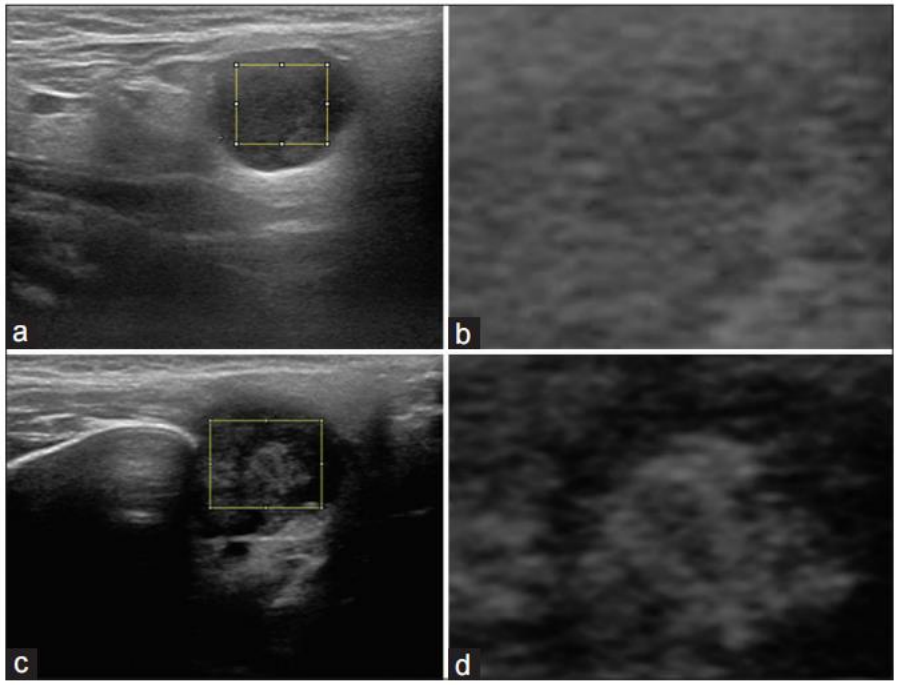

Figure 1: A square block was sampled from a patient with a right parotid tumor (a). A representative US picture was selected for further texture analysis (b). The pathologic report revealed pleomorphic adenoma. Another square block was sampled from a patient with a right parotid tumor with a diagnosis of mucoepidermoid carcinoma (c). Another representative US picture was selected for further texture analysis (d). US: Ultrasound

Multivariate

stepwise logistic regression analysis was further performed to identify four independent factors(including age, intensity, contrast, and entropy) predicting malignant major salivary gland tumors. These four parameters were applied to develop an objective model for the prediction of malignant salivary gland tumors.

The predictive model was as follows: 1.138 ×Age − 1.814 × Intensity + 1.416 × Entropy + 1.714 × Contrast. With the optimal cutoff value of 0.58, the diagnostic performance of this model showed a sensitivity of 83%, specificity of 74%, and overall accuracy of 78% .

JOURNAL OF MEDICAL ULTRASOUND

Home | Current Issue | Previous Issues | For Authors | Published Ahead

CASE REPORT

A Case of Shear Wave Velocity Reflecting the Disease Activity in Glomerulonephritis

Ono, Sayaka; Nishino, Tomohiko*; Takahashi, Kazuhiro; Mimaki, Masakazu

Author Information

Journal of Medical Ultrasound 31(3):p 235-237, Jul–Sep 2023. | **DOI:** 10.4103/jmu.jmu_24_22

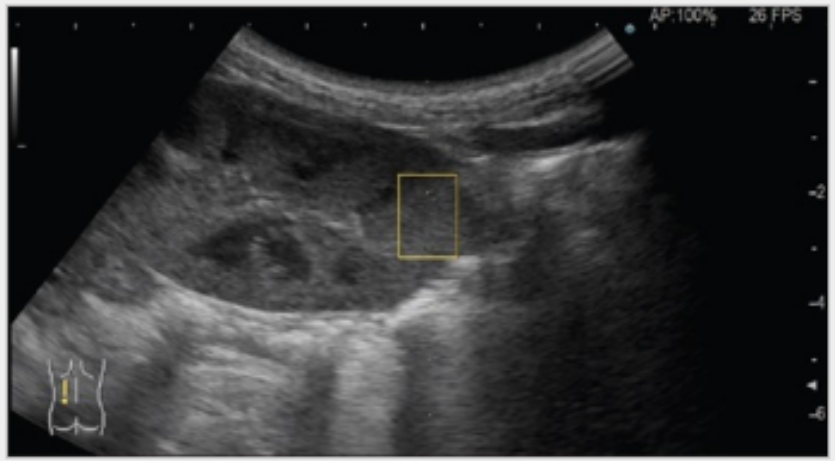

Figure 1: ROI setting and measurement of SWV. The measurement is obtained by lightly applying the probe on the back of the reclining child with as little manual pressure as possible. The region of interest enclosed by the yellow line (10 mm × 15 mm) was determined, while maximally excluding the vasculature and renal pelvis, vertically below the probe. ROI: Region of interest, SWV: Shear wave velocity

SWV was measured four times: once in the acute phase on admission and three times during the recovery period (5, 10, and 13 months later) .

For the measurement, the patient was placed in a prone position, and the kidneys were measured bilaterally at the upper, middle, and lower poles from the back using an ultrasound system (ARIETTA 70, Hitachi Aloka Medical, Japan) and convex probe (1–5 MHz).
SWV was measured ≥50 times at each examination, and the mean was calculated when the net effective SWV was ≥50% [Figure 1]. SWV was significantly lower during the recovery period than in the acute phase, and the values showed reproducibility [Figure 2, $P < 0.02$].

SWV is a noninvasive modality that can reflect disease activity in glomerulonephritis. Notably, in this case, SWV fluctuated according to disease activity. This patient's disease course was similar to that of most PSAGN cases, where remission is spontaneous, and relapse is rare. To the best of our knowledge, no study has performed temporal measurement of SWV in acute glomerulonephritis yet; however, this method may be useful for assessing glomerulonephritis activity.

Case Report

Combination between Dunbar Syndrome and May–Thurner Syndrome: A Rare Case Report

Renato Farina*, Federica Galioto, Davide Castiglione, Antonio Basile

University of Catania, Department of Surgical and Medical Sciences Advanced Technologies GF Ingrassia, Catania, Italy

Abstract

Dunbar syndrome (DS) and May–Thurner syndrome (MTS) are part of a group of rare vascular disorders known as "vascular compression syndromes." Dunbar's syndrome is caused by the median arcuate ligament of diaphragm, which, due to an abnormal course, causes celiac artery compression. MTS is caused by the left common iliac vein compression pushed against the spine by the right common iliac artery causing progressive flow congestion and leading to thrombosis. Ultrasound is the first-level examination for the diagnosis of these rare pathologies and allows to recognize vascular compressions and to obtain an estimate of stenosis degree. We describe a very rare case of DS and MTS combination in a young man with postprandial pain and left lower limb thrombosis.

Keywords: Cardiovascular abnormalities, celiac artery, Dunbar syndrome, May–Thurner syndrome, ultrasound

Case Report

A 38-year-old man was referred for our observation for excessive weight loss (12 kg in 6 months), swelling, and claudication of the left lower limb. The patient underwent CT and US of the left lower limb and abdominal vessels. A CT device (Optima 64 slice, GE Healthcare) and a May Lab "Nine" US device (Esaote Genova), with convex 3–7.5 Mhz and linear 5–14 MHz probe, were used. The study has been performed in forced inspiration and forced expiration

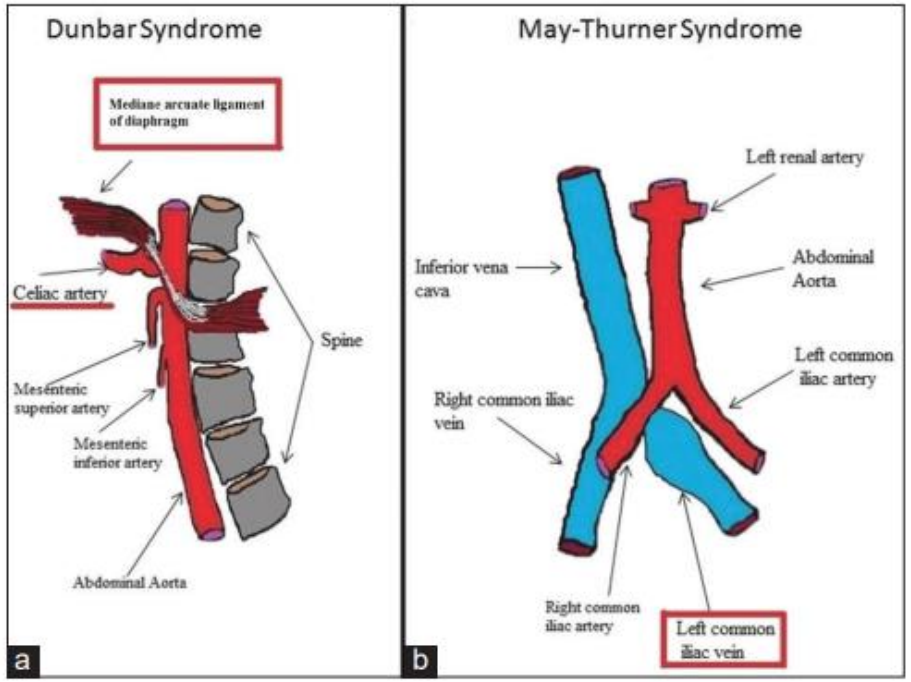

Figure 1: Summary diagram of the anatomical structures involved in patients with Dunbar syndrome and May–Thurner syndrome. (a) Patient with celiac artery compression by the median arcuate ligament. (b) Patient with left common iliac vein compression

Figure 2: CT findings of DS. (a) CT scans in axial view performed in expiratory apnea show celiac artery stenosis at origin (arrow). (b) The CT view in sagittal plane shows the typical DS pattern with "hook" appearance due to celiac artery stenosis (arrow) and poststenotic dilatation. (c) CT scans in axial view show left common iliac vein stenosis caused by the right common iliac artery (short arrow) pushing it against the spine, with thrombosis of the prestenotic tract (long arrow). Left common iliac artery (arrowhead). (d) CT scan in sagittal view shows complete thrombosis of the left common iliac vein (short arrows). Left common iliac artery (long arrow). CT: Computed tomography, DS: Dunbar syndrome

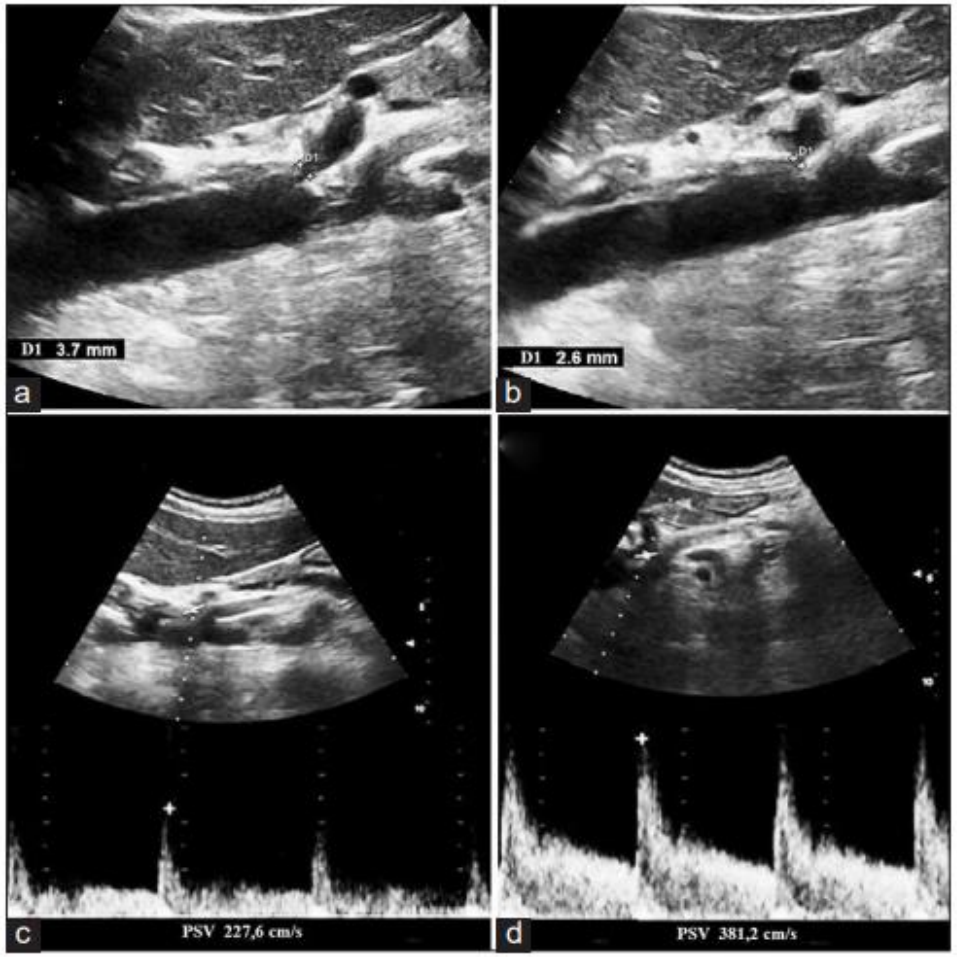

Figure 3: Ultrasound findings of DS. (a) Gray scale ultrasound of the CA, performed in inspiratory apnea, shows a stenosis at origin of CA (3, 7 mm in caliber), (b) which is accentuated in expiratory apnea (2, 6 mm). (c) The flow measurement of CA shows mild increase of peak speed velocity in inspiratory apnea (227,6 cm/s) and significantly increases in expiratory apnea (381,2 cm/s) (d). CA: Celiac artery

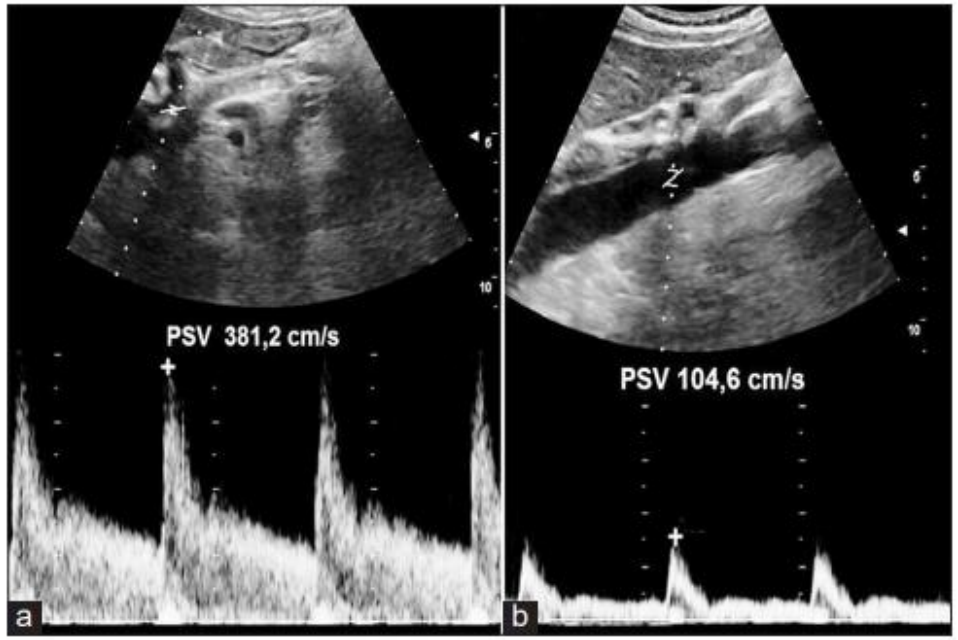

Figure 4: Ultrasound findings of DS. The flow ratio measuration is obtained from ratio between PSV of CA, measured in stenotic tract in expiratory apnea (a) and PSV of abdominal aorta measured at CA origin level (b). DS: Dunbar syndrome, CA: Celiac artery, PSV: Peak speed velocity

Abstract

Objective

The aim of the present study was to illustrate the (potential) diagnostic role of high resolution US images in assessing the elementary lesions of dactylitis.

Methods

Using high-frequency US machines/probes, we matched the micro-anatomical cadaveric architecture of the digit with multiple sonographic findings of dactylitis. High-sensitive color/power Doppler assessments have also been performed to evaluate the digital microvasculature.

Discussion

Modern US equipment/features guarantee prompt and in-depth B-mode and color/power Doppler imaging of tiny anatomical structures of the digit which are usually not properly visible with standard US machines. More specifically, hypervascularization of the digital subcutaneous tissue, fibrous pulleys of flexor tendons, dorsal synovial pads as well as pathological changes of the distal entheseal anchorage network can be accurately detected.

Conclusion

In clinical practice, high-end US equipment can be used to accurately assess the digits in patients with dactylitis. This way, simple and convenient sonographic diagnosis of different elementary lesions can be timely established.

Contents lists available at ScienceDirect

Ultrasound in Medicine & Biology

journal homepage: www.elsevier.com/locate/ultrasmedbio

Review Article

Focused Ultrasound for Dermal Applications

Ahmed M. Al-Jumaily [a,*], Hassan Liaquat [a], Sharad Paul [b]

[a] Institute of Biomedical Technologies, Auckland University of Technology, Auckland, New Zealand
[b] University of Auckland, Auckland, New Zealand

ARTICLE INFO

Keywords:
High-intensity focused ultrasound
Microfocused ultrasound
Skin tightening
Fat reduction
Pigmentary disorder
Skin cancer

Focused ultrasound (FUS) is emerging as one of the most promising, non-invasive treatment techniques. The advancement of transducer technology has paved the way for dermatological applications. A comprehensive review is presented for healthcare practitioners and researchers, summarizing the effect of various operational parameters on the injury zone produced by ultrasound beams for various dermatological applications, which include skin tightening, fat reduction, hyperpigmentation and cancer treatment. In this article, we aim to highlight the efficient operational parameters of FUS to enhance pain relief during surgery and its affordability for skin treatment. Finally, a prospective future technique for efficient FUS is discussed.

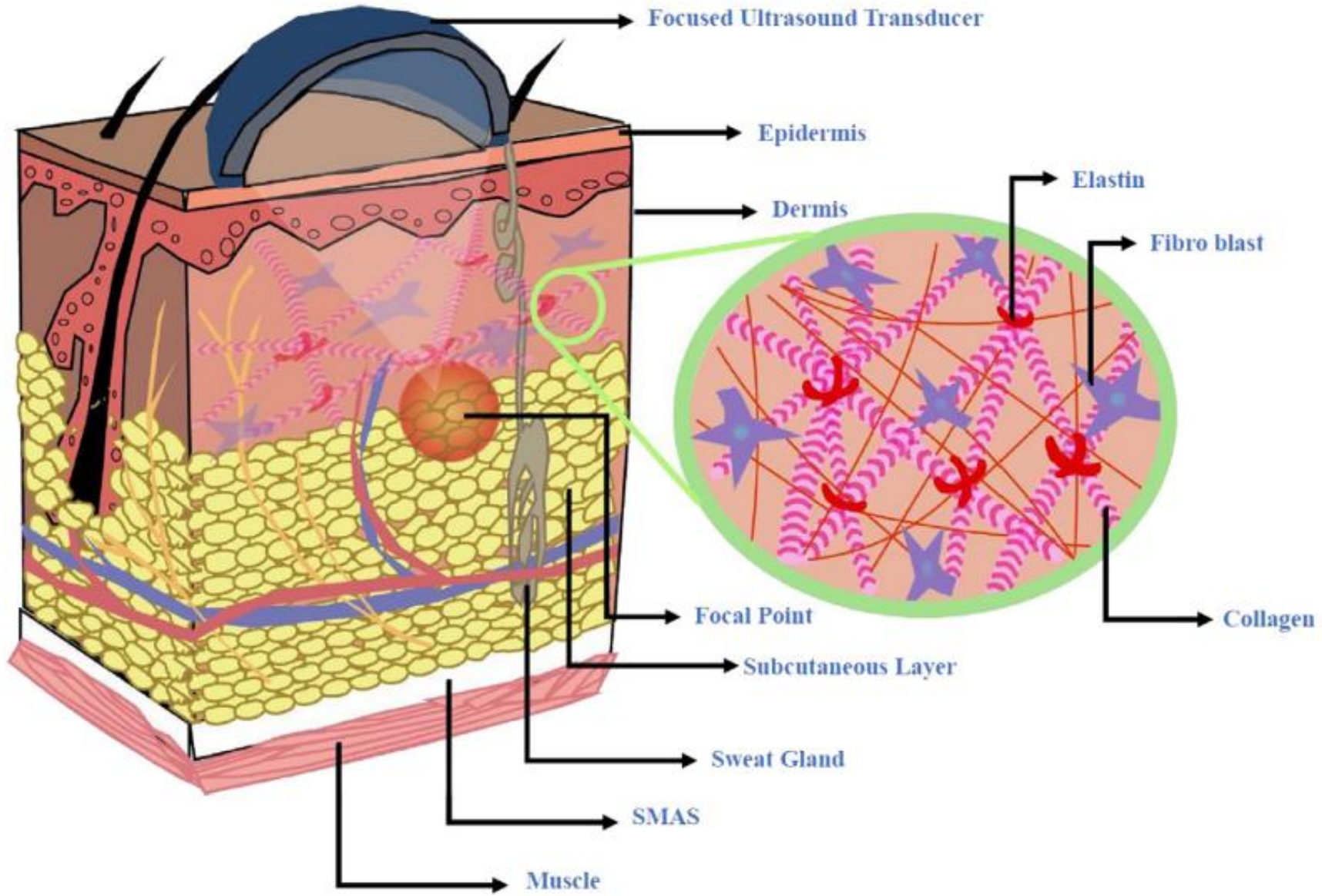

Figure 1. Skin structure and the focused ultrasound.

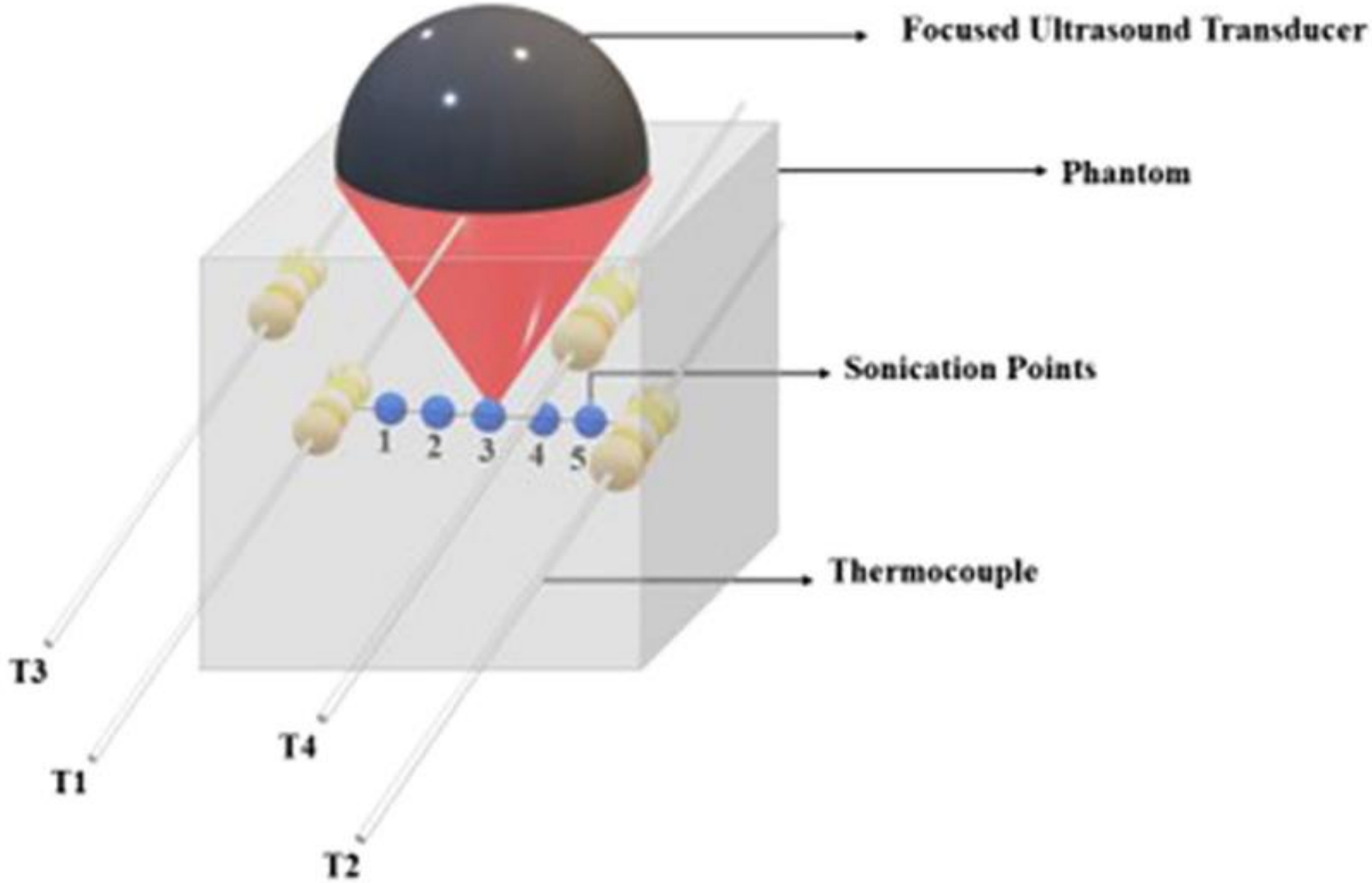

Figure 2. Schematic diagram of the experimental setup used in Dasgupta [57].